Supporting Information for:

Characterizing Intermediates Along the Transition from Polyproline I to Polyproline II Using Ion Mobility Spectrometry-Mass Spectrometry

Liuqing Shi,[†] Alison E. Holliday,[‡] Huilin Shi,[†] Feifei Zhu,[†] Michael A. Ewing,[†] David H. Russell,[§] and David E. Clemmer*,[†]

[†]*Department of Chemistry, Indiana University, 800 Kirkwood Avenue, Bloomington, Indiana 47405, United States*
[‡]*Department of Chemistry and Biochemistry, Swarthmore College, Swarthmore, Pennsylvania 19081, United States*
[§]*Department of Chemistry, Texas A&M University, College Station, Texas 77843, United States*

Table S1. Summary of the Rate Constants (in s^{-1}) of Each Step in the Proposed Mechanism for the Five Explored Temperatures.[a]

rate constant	5 °C	15 °C	23 °C	35 °C	45 °C
k_1	$(3.2 \pm 0.5) \times 10^{-4}$	$(1.3 \pm 0.2) \times 10^{-3}$	$(2.0 \pm 0.2) \times 10^{-3}$	$(7.6 \pm 0.3) \times 10^{-3}$	$(1.9 \pm 0.3) \times 10^{-2}$
k_2	$(7.2 \pm 1.1) \times 10^{-5}$	$(2.4 \pm 0.2) \times 10^{-4}$	$(4.0 \pm 0.3) \times 10^{-4}$	$(2.0 \pm 0.0) \times 10^{-3}$	$(5.0 \pm 0.2) \times 10^{-3}$
k_3	$(1.6 \pm 0.2) \times 10^{-4}$	$(5.1 \pm 0.9) \times 10^{-4}$	$(8.4 \pm 0.8) \times 10^{-4}$	$(4.5 \pm 0.3) \times 10^{-3}$	$(1.3 \pm 0.0) \times 10^{-2}$
k_4	$(1.4 \pm 0.5) \times 10^{-4}$	$(7.1 \pm 1.1) \times 10^{-4}$	$(8.2 \pm 0.4) \times 10^{-4}$	$(4.8 \pm 0.4) \times 10^{-3}$	$(1.6 \pm 0.1) \times 10^{-2}$
k_{5F}	$(2.3 \pm 0.5) \times 10^{-4}$	$(6.7 \pm 0.3) \times 10^{-4}$	$(1.0 \pm 0.3) \times 10^{-3}$	$(4.6 \pm 0.3) \times 10^{-3}$	$(1.1 \pm 0.0) \times 10^{-2}$
k_{5G}	$(1.5 \pm 0.2) \times 10^{-4}$	$(2.9 \pm 0.2) \times 10^{-4}$	$(6.0 \pm 0.5) \times 10^{-4}$	$(2.4 \pm 0.3) \times 10^{-3}$	$(6.4 \pm 1.0) \times 10^{-3}$
k_{5H}	$(5.6 \pm 2.0) \times 10^{-6}$	$(4.4 \pm 1.9) \times 10^{-5}$	$(3.3 \pm 0.8) \times 10^{-5}$	$(3.3 \pm 0.1) \times 10^{-4}$	$(1.2 \pm 0.3) \times 10^{-3}$

[a] The average and standard deviation were obtained from a triplicate analysis.

Table S2. Summary for the Candidate Solution-Phase Structures Prepared in the Simulation.

initial geometry		model geometry Ω_{calc} (Å^2)	
number	*cis*/*trans* peptide bond distribution[a]	lowest-energy geometry	Average values[b]
1	CCCCCCCCCCCC	324	320 ± 6
2	TTTTTTTTTTTT	287	287 ± 6
3	TCCCCCCCCCCC	295	297 ± 5
4	TTCCCCCCCCCC	309	309 ± 4
5	TTTCCCCCCCCC	306	304 ± 5
6	TTTTCCCCCCCC	312	313 ± 12
7	TTTTTCCCCCCC	306	307 ± 5
8	TTTTTTCCCCCC	318	319 ± 9
9	TTTTTTTCCCCC	321	311 ± 6
10	TTTTTTTTCCCC	282	285 ± 4
11	TTTTTTTTTCCC	287	293 ± 9
12	TTTTTTTTTTCC	299	304 ± 4
13	TTTTTTTTTTTC	310	310 ± 3
14	CCCCCCCCCCCT	297	292 ± 3
15	CCCCCCCCCCTT	301	302 ± 5
16	CCCCCCCCCTTT	294	297 ± 3
17	CCCCCCCCTTTT	295	295 ± 7
18	CCCCCCCTTTTT	304	306 ± 3
19	CCCCCCTTTTTT	301	303 ± 6
20	CCCCCTTTTTTT	312	310 ± 6
21	CCCCTTTTTTTT	316	311 ± 9
22	CCCTTTTTTTTT	304	305 ± 4
23	CCTTTTTTTTTT	315	313 ± 4
24	CTTTTTTTTTTT	309	312 ± 6
25	CCCCCTCCCCCC	290	300 ± 7
26	CCCCCTTCCCCC	294	293 ± 2
27	CCCCTTTCCCCC	292	292 ± 3
28	CCCCTTTTCCCC	317	322 ± 9
29	CCCCTTTTTCCC	301	305 ± 3
30	CCCTTTTTTCCC	294	299 ± 4
31	CCTTTTTTTCCC	301	299 ± 4
32	CCTTTTTTTTCC	307	303 ± 6
33	CTTTTTTTTTCC	307	314 ± 4
34	CTTTTTTTTTTC	298	307 ± 6
35	CCCCCCTCCCCC	306	298 ± 6
36	CCCCCTTTCCCC	293	293 ± 4
37	CCCCTTTTTCCC	306	298 ± 9
38	CCCTTTTTTTCC	307	311 ± 8
39	CCTTTTTTTTTC	306	296 ± 8
40	TCCCCCCCCCCT	336	338 ± 6
41	TTCCCCCCCCCT	338	334 ± 7

42	TTCCCCCCCCTT	321	321 ± 4
43	TTTCCCCCCCTT	305	329 ± 17
44	TTTCCCCCCTTT	303	301 ± 4
45	TTTTCCCCCTTT	311	304 ± 5
46	TTTTCCCCTTTT	296	302 ± 3
47	TTTTTCCCTTTT	306	304 ± 3
48	TTTTTCCTTTTT	308	311 ± 4
49	TTTTTTCTTTTT	322	315 ± 6
50	TCCCCCCCCCTT	294	299 ± 3
51	TTCCCCCCCTTT	307	315 ± 6
52	TTTCCCCCTTTT	314	308 ± 9
53	TTTTCCCTTTTT	301	308 ± 7
54	TTTTTCTTTTTT	296	301 ± 4
55	TTCCCTCCCCCC	296	301 ± 10
56	TTCCCCCCCCCT	295	296 ± 4
57	TTCCCTTCCCCC	296	297 ± 5
58	TTTCCTCCCCCC	299	296 ± 6
59	TTTCCCTCCCCC	308	297 ± 9
60	TTTCCCCCTCCC	306	311 ± 17
61	TTTCCCCCCCCT	304	306 ± 5
62	TTTCTTCCCCCC	299	298 ± 5
63	TTTCCTTCCCCC	293	292 ± 2
64	TTTTTTTTCTCC	327	326 ± 8
65	TTTTTTTTCCTC	316	301 ± 7
66	TTTTTTTTCCCT	312	296 ± 5
67	TTTTTTTTTCTC	302	305 ± 3
68	TTTTTTTTTCCT	301	306 ± 4
69	TTTTTTTTTTCT	278	286 ± 10

[a] The *cis*/*trans* peptide bond distribution along the backbone of the initial solution-phase geometry that is prepared in the simulation is given here. “C” represents the *cis* form, and “T” corresponds to the *trans* configuration.
[b] For each model geometry listed here, the average and standard deviation were calculated from the ten lowest-energy conformations.

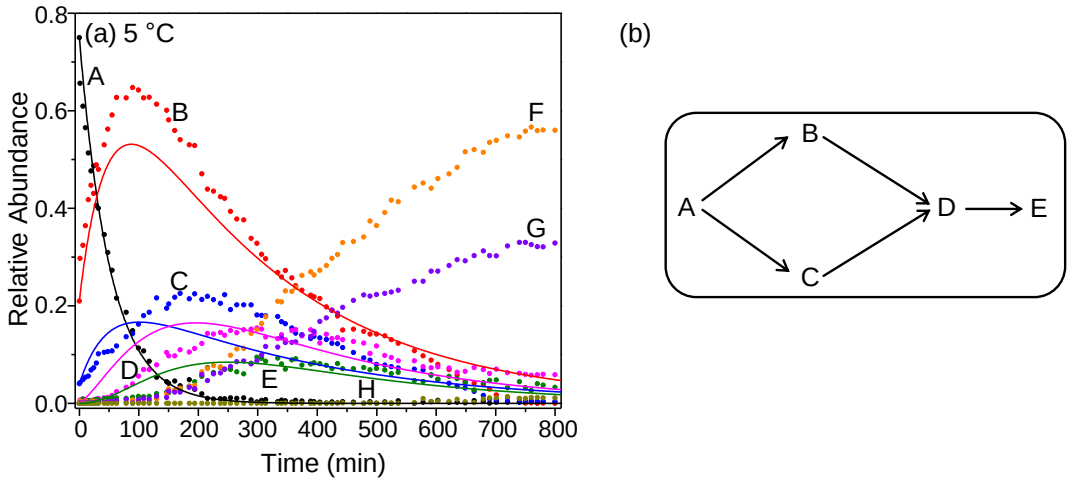

Figure S1. Relative abundance of different conformer types for the transition from PPI to PPII in 10:88:2 1-propanol/H_2O/HOAc (v/v/v) at 5 °C (a) as a function of transition time, and one partial route (b) that does not work for fitting the data points.

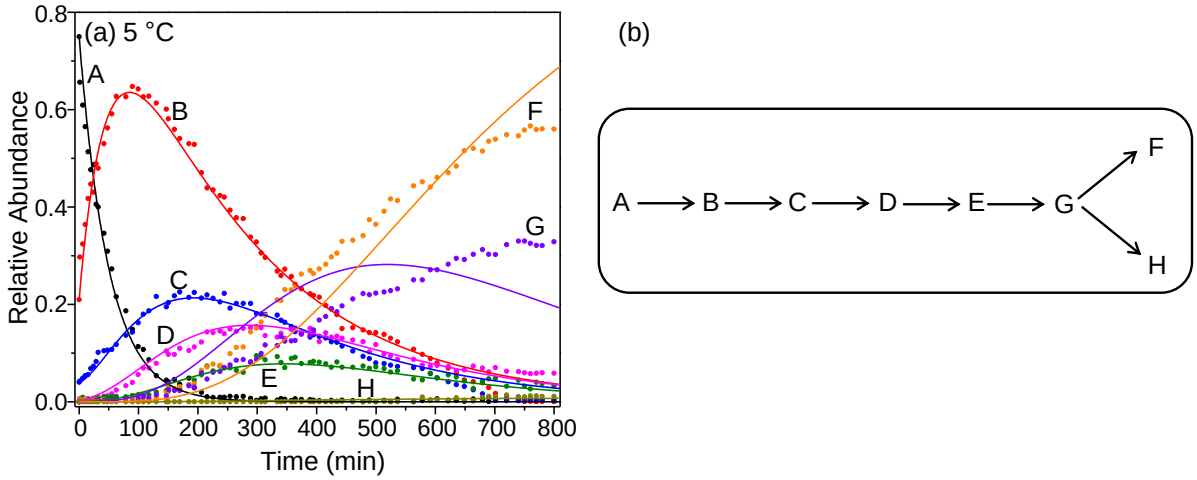

Figure S2. Relative abundance of different conformer types for the transition from PPI to PPII in 10:88:2 1-propanol/H_2O/HOAc (v/v/v) at 5 °C (a) as a function of transition time, and one transition route (b) that does not work for fitting the data points.

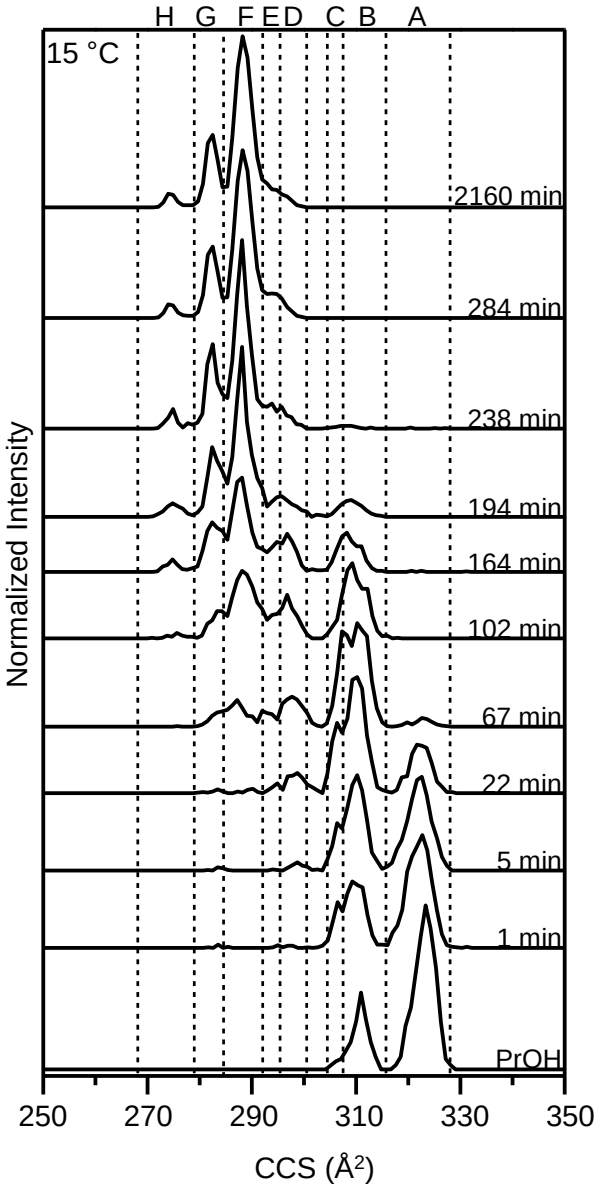

Figure S3. Collision cross section distributions for the $[M+2H]^{2+}$ ions of Pro13 obtained at different transition times, showing the transition from PPI to PPII in 10:88:2 1-propanol/H_2O/HOAc (v/v/v) at 15 °C. In order to illustrate the initial distribution for the transition, the distribution for the ions formed by electrospraying 98:2 1-propanol/HOAc is also shown at the bottom. The transition times when the distributions were obtained are indicated in each trace, and dashed lines delineate the collision cross section region for each conformer type.

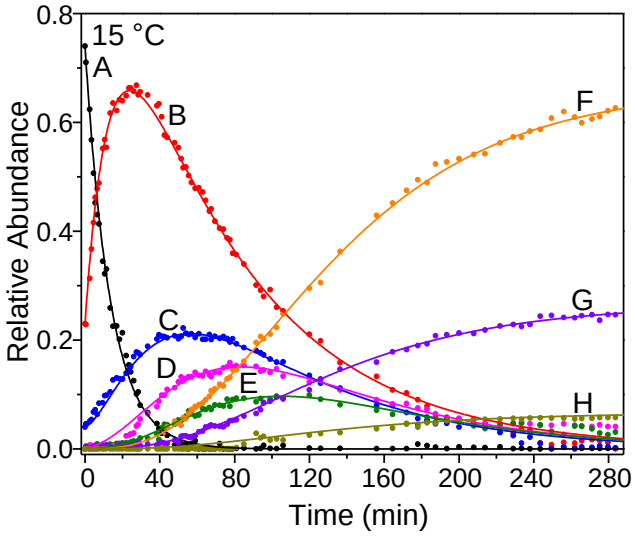

Figure S4. Relative abundance of different conformer types for the transition from PPI to PPII in 10:88:2 1-propanol/H_2O/HOAc (v/v/v) at 15 °C as a function of transition time. The lines show the best fitting results, corresponding to the transition mechanism shown in Figure 2c. Various colors are used to represent different conformations: black is conformer A, red is conformer B, blue is conformer C, magenta is conformer D, olive is conformer E, orange is conformer F, violet is conformer G, and dark yellow is conformer H.

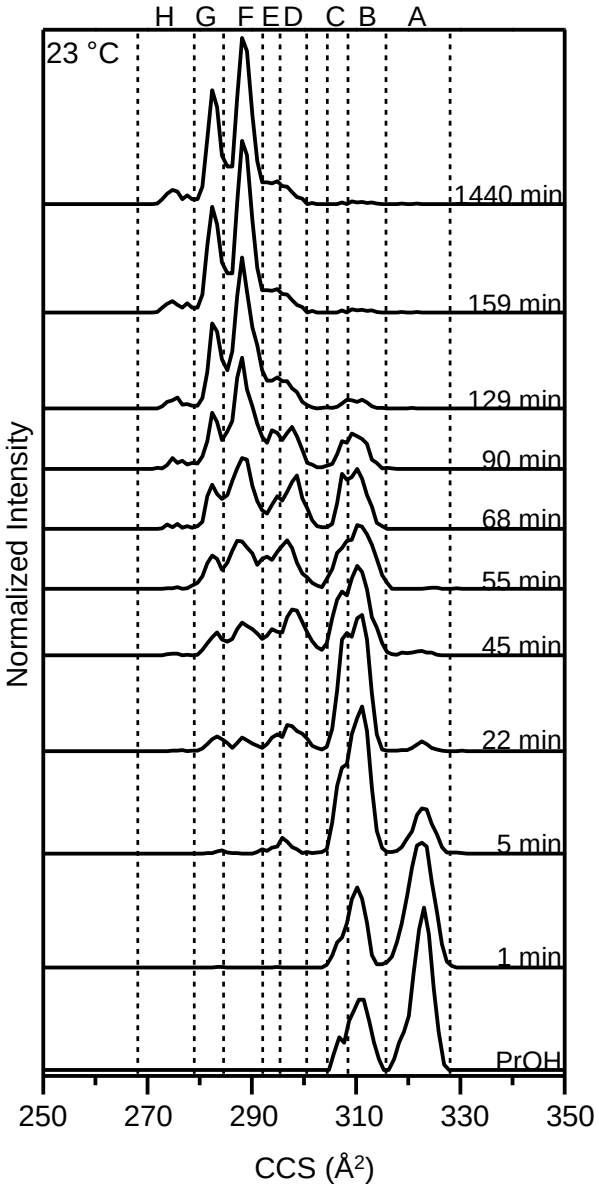

Figure S5. Collision cross section distributions for the $[M+2H]^{2+}$ ions of Pro13 obtained at different transition times, showing the transition from PPI to PPII in 10:88:2 1-propanol/H_2O/HOAc (v/v/v) at 23 °C. In order to illustrate the initial distribution for the transition, the distribution for the ions formed by electrospraying 98:2 1-propanol/HOAc is also shown at the bottom. The transition times when the distributions were obtained are indicated in each trace, and dashed lines delineate the collision cross section region for each conformer type.

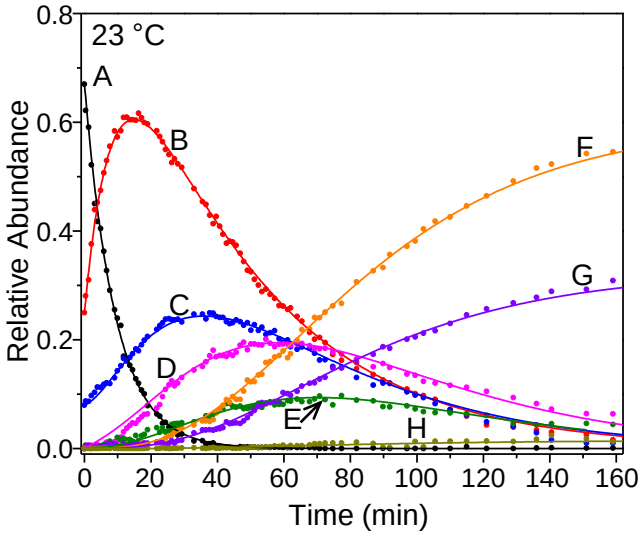

Figure S6. Relative abundance of different conformer types for the transition from PPI to PPII in 10:88:2 1-propanol/H_2O/HOAc (v/v/v) at 23 °C as a function of transition time. The lines show the best fitting results, corresponding to the transition mechanism shown in Figure 2c. Various colors are used to represent different conformations: black is conformer A, red is conformer B, blue is conformer C, magenta is conformer D, olive is conformer E, orange is conformer F, violet is conformer G, and dark yellow is conformer H.

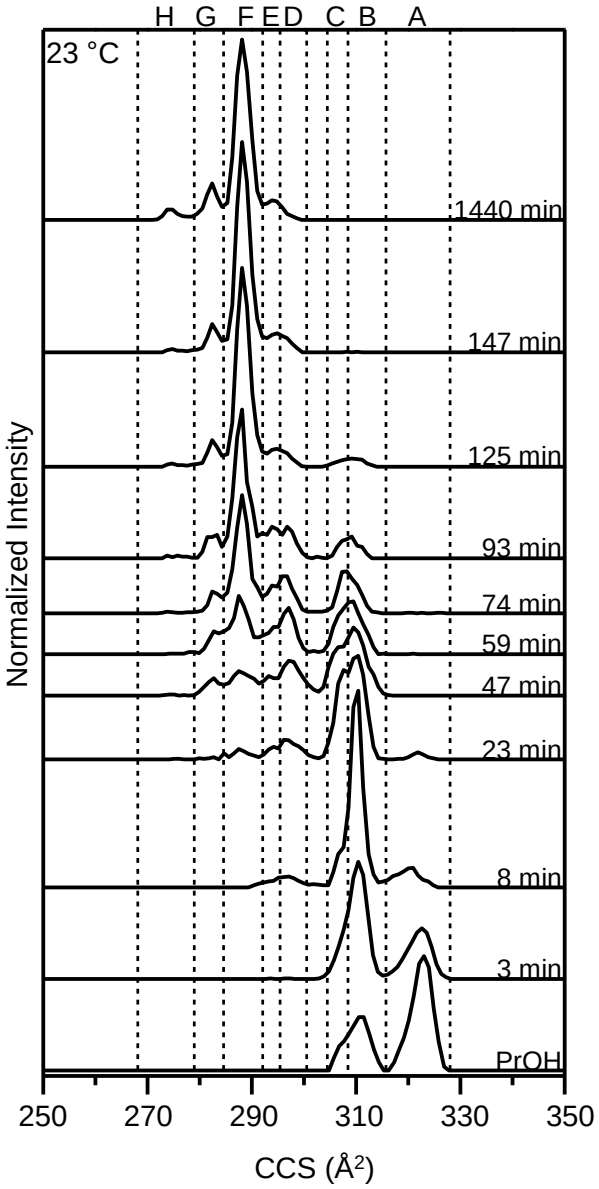

Figure S7. Collision cross section distributions for the $[M+2H]^{2+}$ ions of Pro13 obtained at different transition times, showing the transition from PPI to PPII in the absence of acid (10:90 1-propanol/H_2O (v/v)) at 23 °C. In order to illustrate the initial distribution for the transition, the distribution for the ions formed by electrospraying 1-propanol is also shown at the bottom. The transition times when the distributions were obtained are indicated in each trace, and dashed lines delineate the collision cross section region for each conformer type.

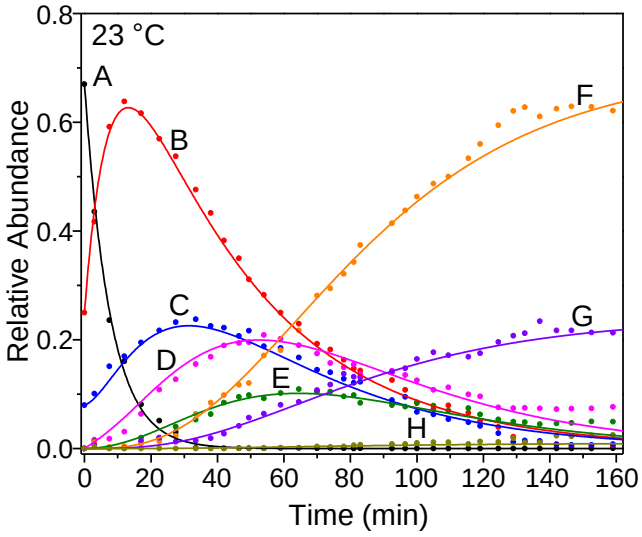

Figure S8. Relative abundance of different conformer types for the transition from PPI to PPII in the absence of acid (10:90 1-propanol/H_2O (v/v)) at 23 °C as a function of transition time. The lines show the best fitting results, corresponding to the transition mechanism shown in Figure 2c. Various colors are used to represent different conformations: black is conformer A, red is conformer B, blue is conformer C, magenta is conformer D, olive is conformer E, orange is conformer F, violet is conformer G, and dark yellow is conformer H.

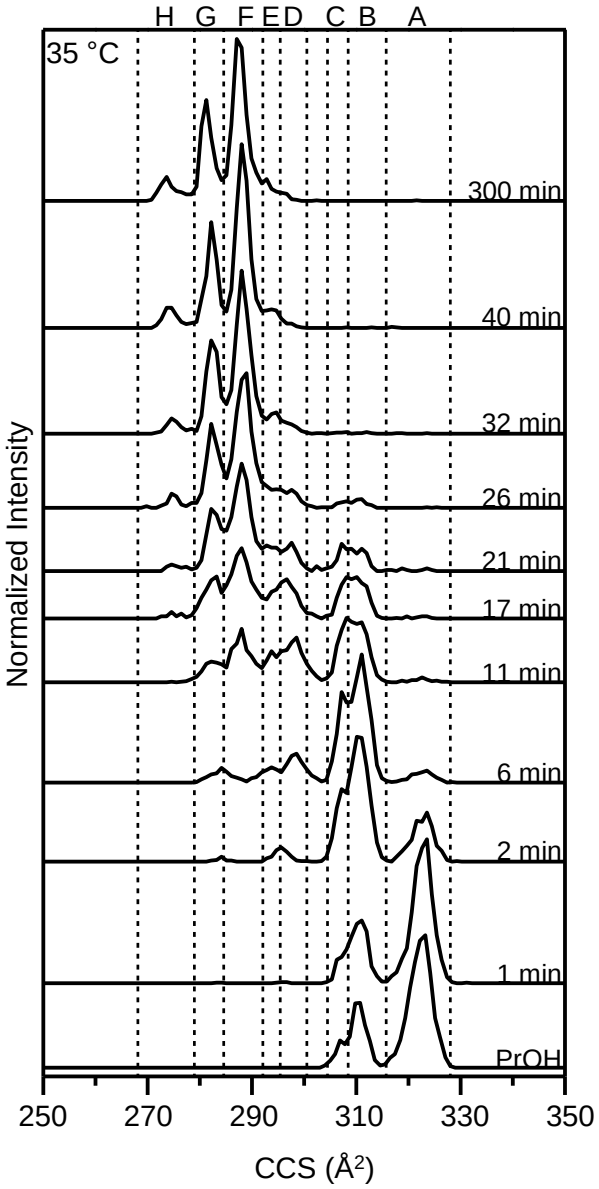

Figure S9. Collision cross section distributions for the $[M+2H]^{2+}$ ions of Pro13 obtained at different transition times, showing the transition from PPI to PPII in 10:88:2 1-propanol/H_2O/HOAc (v/v/v) at 35 °C. In order to illustrate the initial distribution for the transition, the distribution for the ions formed by electrospraying 98:2 1-propanol/HOAc is also shown at the bottom. The transition times when the distributions were obtained are indicated in each trace, and dashed lines delineate the collision cross section region for each conformer type.

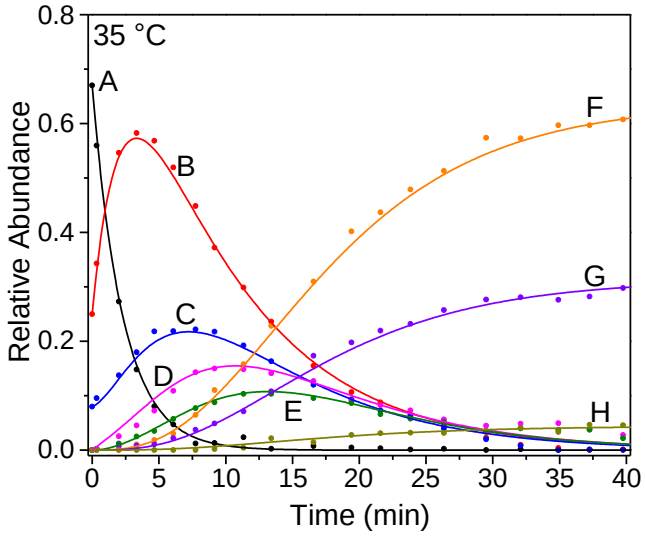

Figure S10. Relative abundance of different conformer types for the transition from PPI to PPII in 10:88:2 1-propanol/H_2O/HOAc (v/v/v) at 35 °C as a function of transition time. The lines show the best fitting results, corresponding to the transition mechanism shown in Figure 2c. Various colors are used to represent different conformations: black is conformer A, red is conformer B, blue is conformer C, magenta is conformer D, olive is conformer E, orange is conformer F, violet is conformer G, and dark yellow is conformer H.